Molecular Therapy
Methods & Clinical Development
Original Article

# Large and small extracellular vesicles from Wharton's jelly MSCs: Biophysics, function, and strategies to improve immunomodulation

July Constanza Buitrago,[1,2,4] Mónica Cruz-Barrera,[1] Valerie Dorsant-Ardón,[1] Carlos Medina,[1] David G. Hernández-Mejía,[1] Karl Beltrán,[1] Natalia Flórez,[3] Bernardo Camacho,[1] Jens Gruber,[2] and Gustavo Salguero[1]

[1]Advanced Therapies Unit, Instituto Distrital de Ciencia Biotecnología e Innovación en Salud – IDCBIS, Bogotá, Colombia; [2]Curexsys GmbH, Göttingen, Germany; [3]Faculty of Medicine, Universidad EAN, Medellín, Colombia; [4]PhD Biomedical and Biological Sciences Program, School of Medicine and Health Sciences, Universidad del Rosario, Bogotá, Colombia

**Extracellular vesicles (EVs) have emerged as mediators of immunosuppression and pro-regenerative processes, particularly through mesenchymal stromal cells (MSCs) across various disease models. Despite significant progress, there is still a need for a deeper understanding of EV content and functionality to fully harness their biomedical potential. Moreover, strategies to enhance EV production for clinical scalability are still under development. This study aimed to characterize two distinct types of EV—large EV (lgEV) and small EV (smEV)—secreted by Wharton's jelly MSCs (WJ-MSCs). Strategies were explored to augment both EV production and their immunoregulatory effects. Both lgEV and smEV displayed typical EV markers and demonstrated inhibition of human lymphocyte proliferation. Furthermore, analysis of IsomiR content revealed a pronounced immunomodulating signature within MSC-derived EVs, validated by a dual-fluorescence reporter system. MSC primed with pro-inflammatory cytokines yielded increased production of lgEV and smEV, enhancing their immunomodulatory potency. Finally, genetically engineering WJ-MSC to express CD9 resulted in lgEV and smEV with heightened efficacy in suppressing lymphocyte proliferation. This study successfully isolated, characterized, and demonstrated the potent immunosuppressive effect of WJ-MSC-derived lgEV and smEV. We propose cytokine preconditioning and genetic manipulation as viable strategies to enhance the therapeutic potential of WJ-MSC-derived EV in inflammatory conditions.**

## INTRODUCTION

Human umbilical cord-derived Wharton's jelly mesenchymal stromal cells (WJ-MSCs) have been found to have potent clinical applications due to their strong immunomodulatory effects via cell-to-cell interactions and release of soluble factors and extracellular vesicles (EVs).[1–3] EVs are a family of small membrane-bound nanoparticles that carry a wide range of biomolecules, including proteins, lipids, nucleic acids, and small molecules.[4] EVs can be classified based on their size and biogenesis pathway, including exosomes, microvesicles, and apoptotic bodies.[5] Exosomes are 30- to 100-nm particles that emerge from intraluminal endosomal multivesicular bodies that mature and fuse with plasma membrane following the exocytic pathway.[6] Microvesicles are generated by plasma membrane protrusions followed by fission of their membrane stalk.[5] Recently, these two EV types were also classified as small (smEV) and large (lgEV), respectively. Finally, apoptotic bodies are 50- to 5,000-nm EVs released during cell apoptosis.[7,8] Interestingly, EVs play important roles in various physiological and pathological processes, such as cell-to-cell communication and immune regulation, and are thought to be involved in the progression of several diseases, including cancer, neurodegenerative diseases, and cardiovascular diseases.[9–11] Despite that MSC-derived EVs seem to play a key role in immunomodulatory processes and therefore are a candidate for biomedical use, technologies to develop EV as therapeutic tools are in the early stages and need to be researched further.

Proposed mechanisms by which MSC-EV induce immunomodulatory responses involve the transfer of microRNAs (miRNAs) to recipient cells.[12] There are several mechanisms by which miRNAs can be loaded into EVs, including the endosomal pathway, in a process regulated by Argonaute, Dicer, and tetraspanins. The latter two play important roles in the synthesis, processing, and sorting of miRNAs into EVs.[13] Of note, EVs are enriched with tetraspanins such as CD9, CD63, and CD81 and proteins like syntenin-1, ALG-2-interacting protein X (Alix), and tumor susceptibility gene 101.[8] Among these, CD9 is thought to be critically involved in the regulation of EV biogenesis, modulation of vesicular uptake and degradation, and transfer of biomolecular cargos to recipient cells.[14–16] In this regard, gene transfer strategies to explore the role of CD9 in WJ-MSC EVs could provide an attractive approach to improve EV function for further biomedical applications.

Received 29 February 2024; accepted 4 October 2024;
https://doi.org/10.1016/j.omtm.2024.101353.

**Correspondence:** Jens Gruber, Curexsys GmbH, Göttingen, Germany.
**E-mail:** jens.gruber@curexsys.com
**Correspondence:** Gustavo Salguero, Advanced Therapies Unit, Instituto Distrital de Ciencia Biotecnología e Innovación en Salud – IDCBIS, Bogotá, Colombia.
**E-mail:** gsalguero@idcbis.org.co

In this study, we characterized lgEVs and smEVs secreted by WJ-MSC in terms of membrane markers, immunosuppression, and miRNA profile. We additionally explored the impact of MSC priming with pro-inflammatory cytokines (CKs) and the CD9 overexpression in MSCs on the production and anti-inflammatory effect of the MSC-EV. We suggest that subsequent functional studies will reveal mechanisms of action in immunomodulation and inflammation processes.

## RESULTS

### Biological and functional characterization of EVs from WJ-MSC

Characterization of WJ-MSC ($n$ = 3–4 donors) was performed according to the International Society for Cellular Therapy criteria. Immunophenotype was evaluated by flow cytometry and differentiation (osteogenic, adipogenic, and chondrogenic) assays. All WJ-MSC donors exhibited a characteristic spindle-shaped morphology and displayed typical MSC phenotypes as evaluated by the high expression of CD90, CD73, and CD105, and absence of hematopoietic markers HLA-DR, CD45, and CD34 (Figure S1A). Similarly, we confirmed differentiation of cells into adipocytes, chondrocytes, and osteocytes by positive staining with oil red, Alcian blue, and alizarin red S, respectively (Figure S1B). To assess the immunomodulatory capacity of WJ-MSC, we conducted functional immunoassays and measured the suppressive potential on $CD3^+$ T cell proliferation upon phytohemagglutinin (PHA) stimulation. As expected, WJ-MSC significantly inhibited the proliferation of PHA-activated $CD3^+$ T cells (>100% vs. unstimulated controls; Figure S1C). To establish diverse methodologies for EV isolation, conditioned medium (CM) was collected from WJ-MSC after 48 h in culture with serum deprivation (starvation). Two fractions of EV, lgEVs and smEVs, were evaluated (Figure 1A). Regarding lgEV fraction, we observed a mean size of 298 ± 53 nm or 318 ± 23 nm (Figure 1B) and $9.66x \times 10^9 \pm 7.25 \times 10^9$ or $1.22 \times 10^{10} \pm 2.84 \times 10^9$ total particles upon 30- or 60-min centrifugation, respectively (Figure 1C). For the smEV fraction, we obtained mean sizes of 200 ± 9 nm and 225 ± 11 nm (Figure 1B) from polyethylene glycol (PEG) and ultracentrifugation (UC), respectively. Similarly, particle yield within the smEV fraction averaged $1.71 \times 10^{10} \pm 6.89 \times 10^{10}$ and $9.19 \times 10^9 \pm 2.24 \times 10^9$ total particles (PEG and UC, respectively; Figure 1C). The expression of EV markers (Alix and CD81) in WJ-MSC-derived EV was confirmed by western blot. A low level of apolipoprotein AI (ApoAI), a common contaminant in EV preparations, was also detected (Figure S1D). Similarly, scanning electron microscopy confirmed the morphology and size of EV preparations (Figure S1D). We further assessed the expression of tetraspanins CD9, CD81, and CD63 and the MSC marker CD73 in lgEV and smEV membranes by flow cytometry (Figure 1D). Overall, lgEV displayed no significant differences in expression levels among the three markers regardless of centrifugation time. Similarly, the same expression pattern was observed in CD63 and CD81 in smEV isolated by PEG and UC. In contrast, higher enrichment of CD9 in smEV was observed in PEG-treated preparations as compared to UC. As expected, MSC marker CD73 showed a higher expression in the lgEV compared to the WJ-MSC-smEV fraction. Finally, we assessed the impact of distinct isolation methods on the immunomodulatory potential of lgEV and smEV. Here, adult peripheral blood mononuclear cells (PBMCs) from healthy donors were stimulated with the mitogen PHA and co-cultured with different volumes of WJ-MSC-lgEVs or -smEVs for 5 days. In all experiments, PHA-stimulated T cells showed a 4.5-fold average proliferation as compared to unstimulated controls. Remarkably, both lgEV and smEV treatment inhibited PHA-mediated T cell proliferation in a dose-dependent manner (Figure 1E). WJ-MSC-derived lgEVs and smEVs suppressed T cell proliferation, reaching 29% and 41% of inhibition, respectively, with no statistical differences between isolation protocols. Thus, the methodologies for EV isolation tested here revealed clear advantages regarding recovery and purity of lgEVs and smEVs from WJ-MSC cultures, displaying consistent and expected values in terms of size and yield, hence supporting the feasibility of EV isolation from WJ-MSCs. For further studies, we used 60-min centrifugation for lgEV and PEG precipitation for smEV isolation. Importantly, EVs isolated from WJ-MSCs proved to be potent suppressors of T cell proliferation in a dose-dependent manner.

### sRNA content and differential expression of IsomiR in WJ-MSC-derived EVs

To provide a comprehensive overview of small non-coding RNA expression profiles carried by lgEVs and smEVs derived from WJ-MSCs, we further studied small RNA (sRNA) content present in WJ-MSC-lgEVs and -smEVs by next-generation sequencing (NGS). Total RNA was extracted from lgEVs and smEVs. In addition, we compared sRNA expression profiles present on EVs (vesicular RNA) and compared them with the respective WJ-MSC producer cells (cellular RNA) growing in DMEM supplemented with fetal bovine serum (FBS; normal condition, control [Ctrl]) or without FBS (starvation, Stv) (Figure 2A). Bioinformatic analysis revealed the differential expression of sRNA species in EV (lg and sm) fractions and EV-producer cells (Ctrl and Stv), suggesting specific enrichment patterns of sRNA in WJ-MSC-EV (Figure 2B). Different types of RNA proportions revealing enrichment of rRNA fragments, tRNA, and small non-coding RNAs such as Y RNA in the vesicular samples and indistinctly in the two isolated fractions, lgEV and smEV (Figure 2B). In line with these findings, Baglio et al. demonstrated that the most abundant and enriched sRNAs in adult MSC exosomes are defined tRNA species.[17] Additional studies performing analyses of RNA from EVs have demonstrated that EVs also contain a large variety of other small non-coding RNA species, including RNA transcripts overlapping with protein coding regions, repeat sequences, structural RNAs, tRNA fragments, vault RNA, Y RNA, and small interfering RNAs. Interestingly, many RNAs that were isolated with EVs were found to be enriched in these nanoparticles relative to the RNA profiles of the parental cells.[4,18–20] Among sRNAs present in cellular samples, miRNA was the most frequent sRNA type observed, being 76% ± 3% and 73% ± 2.4% in Ctrl or Stv WJ-MSC cultures, respectively. Meanwhile, WJ-MSC-lgEV and -smEV miRNA content was only 9.8% ± 5.7% and 3.8% ± 2% ($p > 0.05$, smEV vs. lgEV) (Figure 2C). Nevertheless, the distribution of both mature and precursor miRNAs was homogeneous among samples in all experimental groups evaluated. Unsupervised clustering and correlation analysis based on overall miRNA content showed that

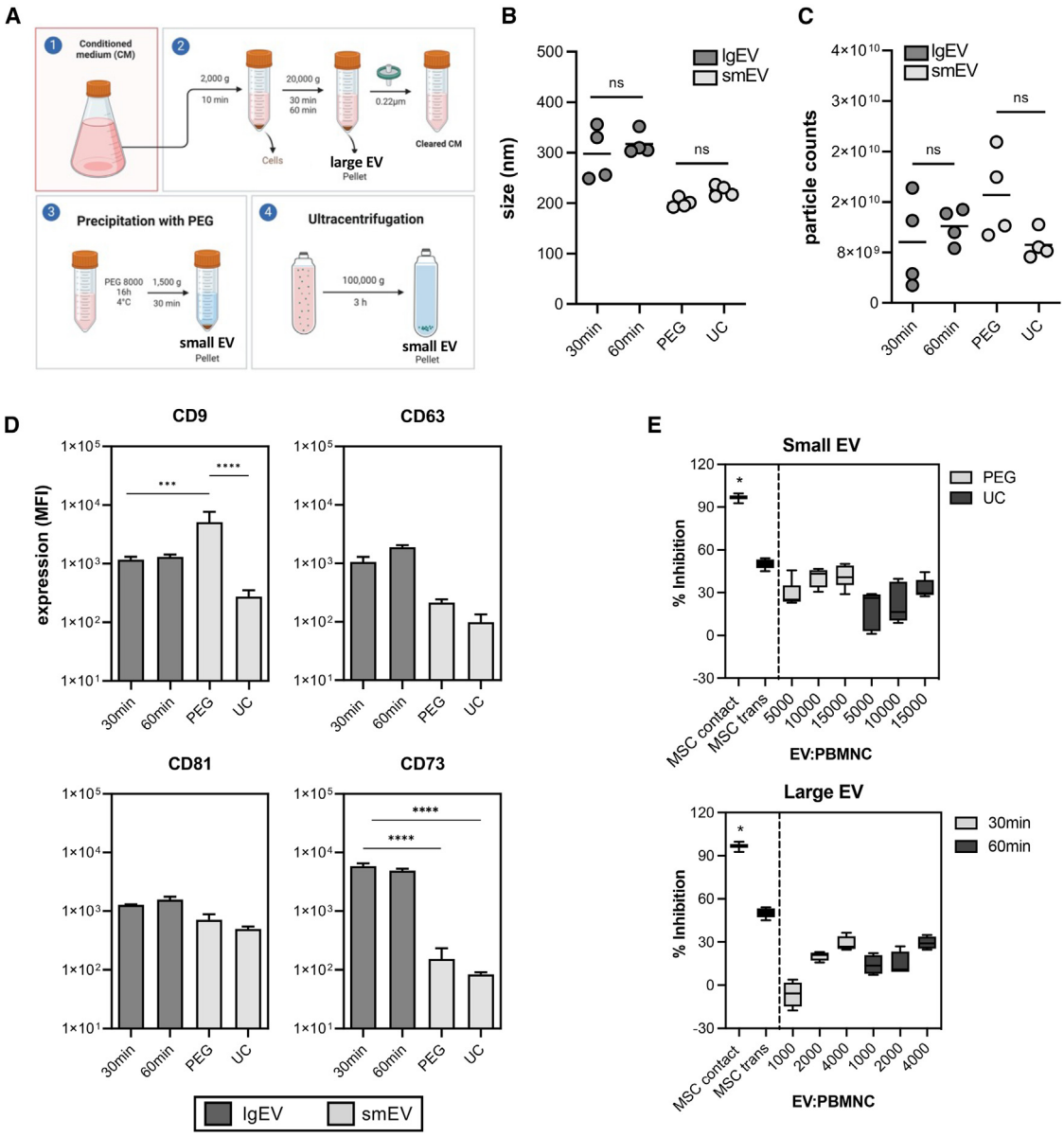


**Figure 1. Characterization of WJ-MSC derived-extracellular vesicles**

(A) Experimental scheme of large EV (lgEV) and small EV (smEV) isolation from WJ-MSC conditioned medium (CM). After reaching confluence, cells were cultured under starvation for 48 h and CM was collected (step 1). lgEVs were isolated from CM by centrifugation (20,000 × *g*, 30 or 60 min) (step 2). smEVs were isolated from filtered CM by precipitation with polyethylene glycol (PEG) (step 3) and ultracentrifugation (UC) (step 4). (B) Size distribution of lgEVs and smEVs derived from WJ-MSC measured by nanoparticle tracking analysis (NTA). Size distribution is displayed as the mean of four donors. (C) lgEV and smEV counts measured by NTA. The number of particles is displayed as the mean of four donors. (D) Mean fluorescence intensity (MFI) for CD9, CD63, CD81, and CD73 expression in lgEVs and smEVs derived from WJ-MSC, measured by fluorescence-activated cell sorting. Data are displayed as a mean of four donors. ***$p < 0.0005$; ****$p < 0.0001$. Error bars represent SDs. (E) Inhibitory effect of lgEVs and smEVs on T cell proliferation. PHA-treated PBMCs were cultured with different ratios of lgEVs ($1 \times 10^3$, $2 \times 10^3$, and $4 \times 10^3$: PBMCs) and smEVs ($5 \times 10^3$, $1 \times 10^4$, and $1.5 \times 10^4$: PBMCs). After 5 days, T cells were collected and stained with anti-CD3 antibody, and absolute counts were determined by flow cytometry using CountBright Absolute Counting Beads. Mean ± SD of four technical replicas. *$p < 0.05$; ***$p < 0.0005$.

EV samples had greater variability ($0.75 < r < 0.90$) as compared to cellular miRNAs, where high similarity ($0.89 < r < 0.96$) was observed. These results point to a weak correlation between cells and EV miRNA profiles (Figure S2A). Finally, to explore the differential expression of miRNA in all groups, DESeq, DESeq2, NOISeq, and Student's t test methods were carried out. To increase astringency in the selection criteria of differentially expressed miRNA, we selected miRNAs that were efficiently detected in at least two methods

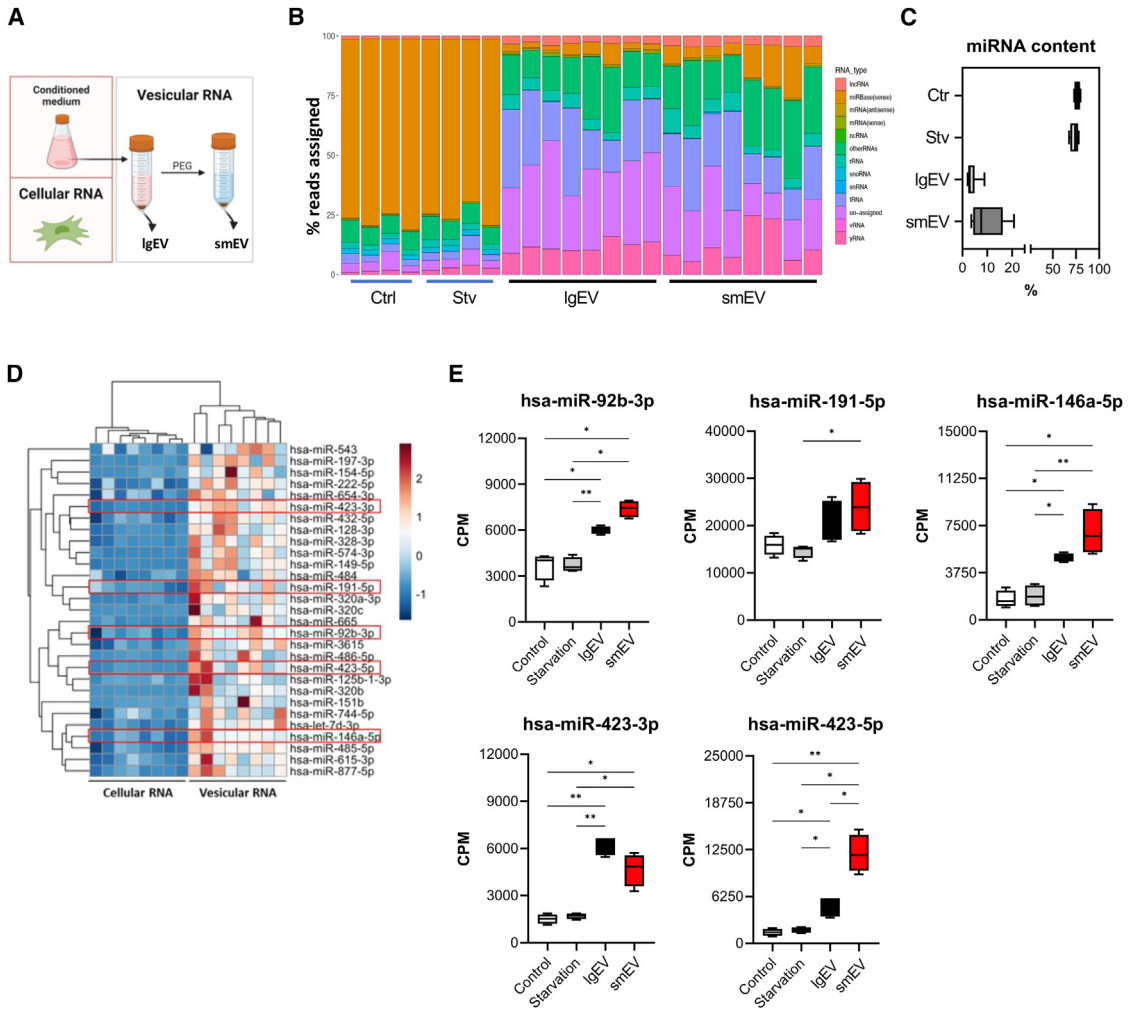


**Figure 2. sRNA content in WJ-MSC-derived EVs**

(A) Experimental approach for sRNA characterization. "Vesicular RNA" indicates sRNA isolated from EVs. WJ-MSCs were cultured under starvation conditions for 48 h. Subsequently, EVs were isolated from CM using PEG, and sRNA was sequenced by NGS. "Cellular RNA" indicates sRNA isolated from the corresponding EV-producer cells, growing in DMEM supplemented with (normal condition or control, Ctrl) or without FBS (starvation, Stv). (B) Distribution of short RNA types, mapping diversity of small non-coding RNA contained in cellular (Ctrl and Stv) and vesicular WJ-MSC samples (lgEVs and smEVs). EVs display different proportions of RNA types as compared with their corresponding cellular RNA. (C) Frequency of miRNA in cellular and vesicular samples. (D) Heatmap depicting normalized counts of the top 30 most abundant IsomiR in lgEVs and smEVs regarding cellular RNA from the starvation and normal cultured WJ-MSC. (E) Counts of miRNA per million of differentially expressed miRNA present in WJ-MSC-derived lgEVs and smEVs. Data are represented as mean ± SD. $^{*}p < 0.05$; $^{**}p < 0.01$.

(Figure S2B). Previously reported EV-associated miRNAs that also showed differential expression here were included within the top 30 miRNAs most significantly enriched in cellular and vesicular samples (Tables 1 and S2). Interestingly, we detected several miRNAs that were selectively transferred to both lgEVs and smEVs and were not enriched in producer cells, as shown by hierarchical cluster analysis (Figure 2D). We identified the top five IsomiRs enriched in WJ-MSC-EV (both lgEV and smEV): miR-92b-3p, miR-191-5p, miR-146a-5p, miR-423-3p, and miR-423-5p (Figure 2E). We introduced additional evidence on sRNA expression profiles present in distinct EV types derived from WJ-MSCs. Based on miRNA species observed in EVs and their respective producer cells, there is strong evidence pointing to differential miRNA enrichment in both WJ-MSC lgEVs and smEVs. We subsequently performed miRNA target analyses, construction of an miRNA/gene network and functional enrichment using the MIENTURNET analysis platform for the selected miRNA derived from WJ-MSC-lgEVs and smEVs. We note that selected miRNAs, such as miR-146, miR-191, miR423-3p, and miR-92, but not miR423-5p, contributed to wide network interactions with predicted targets, as evaluated by miRTarBase (Figure 3A). All miRNA targets appearing in the network are presented as dot plots, as is the corresponding miRNA that recognizes the target. PA2G4, FKB4P, RPL3, IRAK1, HSPA1B, RPS2, FASN, COX1, RRP1, NOTCH2, TMEM33, RAD21, PABPC1, KIF1A, and POLR3H genes were identified as

**Table 1. miRNAs described in MSCs or MSCs-derived EVs**

| miRNA | MSC source | Conclusions | Reference |
|---|---|---|---|
| miRNA-128-3p | hUCMSC-derived Exo | hUCMSC-derived exosomes with hsa-miRNA-128-3p could suppress the proliferation, invasion, and migration of PANC-1 cells *in vitro*; hsa-miRNA-128-3p could be considered as a potential therapy for pancreatic cancer | Xie et al.[21] |
| miR-486-5p | hBM-MSC and ASC-derived Exo | top 4 miRNAs enriched in MSC-EVs compared to MSC | Baglio et al.[17] |
| miR-125b | hUCMSC-derived Exo | essential in suppressing myofibroblast formation by blocking the transforming growth factor β2/SMAD2 pathway in wound healing | Fang et al.[22] |
| miR-543 | unspecified human MSC-derived Exo | hMSCs-Exo facilitates the proliferation, migration, invasion, and angiogenesis of cardiac microvascular endothelial cells through transferring miR-543 | Yang et al.[23] |
| miR-197-3p | hAM-MSC | top 5 miRNAs regulated at both 7 and 14 days after osteogenic induction, suggesting a role in coordinated guidance of osteoblastic differentiation | Avendaño-Felix et al.[24] |
| miR-154-5p | hASC | miR-154-5p negatively regulates ADSC osteogenic differentiation through the Wnt/PCP pathway by directly targeting Wnt11 | Li et al.[25] |
| miR-222-5p | hWJ-MSC | MSC differentiation into SMCs is regulated by miR-503 and miR-222-5p and yields functional SMCs for use in vascular grafts | Gu et al.[26] |
| miR-432-5p | iPSC-MSC | iPSC-MSC secrete exosomes that contain miR-432-5p, which suppresses TRAM2, a vital modulator of the collagen biosynthesis in the corneal stromal stem cells to avert the deposition of ECM | Tang et al.[27] |
| miR-128-3p | BM-MSC | miR-128-3p regulated the TNF-α-induced inflammatory response in BMSC | Wu et al.[28] |
| miR-328-3p | ASC | repression of miR-328-3p in ASC significantly reduced ALP activity during osteogenic differentiation but did not affect calcium deposition | Weilner et al.[29] |
| miR-574-3p | hWJ-MSC<br>unspecified hMSC | combined transfection of 3 miR (miR-106a, miR-574-3 p, and miR-451) will lead to fast and safe UC-MSC-differentiated functioning hepatocytes via a non-viral transfection method<br>manipulating miR-574-3p levels both *in vitro* and *in vivo* inhibited chondrogenesis, suggesting that miR-574-3p might be required for chondrocyte lineage maintenance | Khosravi et al.[30]<br>Guérit et al.[31] |
| hsa-miR-665 | hBMSC-derived Exo | IFN induced a significant increase in 5 miRNAs: hsa-miR-25-3p, hsa-miR-106a-5p, hsa-miR-126-3p, hsa-miR-451a, and hsa-miR-665 | Peltzer et al.[32] |
| miR-486-5p | hUCMSCs-EV | 5 highly enriched miRNA were found: hsa-miR-122-5p, hsa-miR-148a-3p, hsa-miR-486-5p, hsa-miR-let-7a-5p, and hsa-miR-100-5p by high-throughput sequencing of miRNA | Li et al.[33] |

ADSC, adipose-derived stem cells; ALP, alkaline phosphatase; ECM, extracellular matrix; EV, extracellular vesicle; Exo, exosomes; hAM, human amniotic membrane; hASC, human adipose-derived stromal cell; hBMSC, human bone marrow stromal cell; hUCMSC, human umbilical cord mesenchymal stem cell; hWJ, human Wharton's jelly; IFN, interferon; iPSC, induced pluripotent stem cell; miRNA, microRNA; MSC, mesenchymal stromal cell; SMC, smooth muscle cell; TNF-α, tumor necrosis factor-α; TRAM2, translocation-associated membrane protein 2.

the most frequent targets for miRNA enriched in WJ-MSC-EVs (Figure 3B). Finally, enrichment analysis of selected miRNA targets was explored using the Kyoto Encyclopedia of Genes and Genomes, Reactome, WikiPathways, and Disease Ontology pathway (Figures 3C and 3D; Table S3).

To verify the biological activity linked to miRNAs enriched in WJ-MSC-derived EV fractions, we used the untranslated trans assay (UTA) dual-fluorescence reporter system,[34] where the cyan fluorescent protein (CFP) gene carries a selected miRNA complementary sequence that, if present, alters its fluorescence level (Figure 4A). Briefly, UTA expression plasmids (pUTA) were constructed by inserting complementary regions for miR-146a-5p, miR-423-3p, miR-423-5p, miR-92b-3p, and miR-191-5p within the 3′ UTR of CFP. For functional experiments, human HEK293 cells were incubated with WJ-MSC lgEVs, smEVs, or control media for 24 h. Subsequently, cells were independently transfected with five different sensor constructs, and CFP/YFP (yellow fluorescent protein) expression was evaluated after 72 h. $YFP^+$ cells were gated, and the ratio between log (CFP) and log (YFP) was calculated. Since YFP and CFP fluorescence levels are proportional in the absence of miRNA repression, deviation from the linearity of fluorescence intensity from CFP related to YFP indicated the positive target of the evaluated IsomiR. In miR-92b-3p and miR-191-5p targeted constructs, CFP fluorescence faded as compared to YFP in the presence of lgEVs or smEVs (Figure 4A). Interestingly, the miR-191-targeted construct decreased the CFP/YFP ratio after treatment of both vesicular fractions (lgEVs and smEVs), whereas the miR-92-targeted construct showed a higher

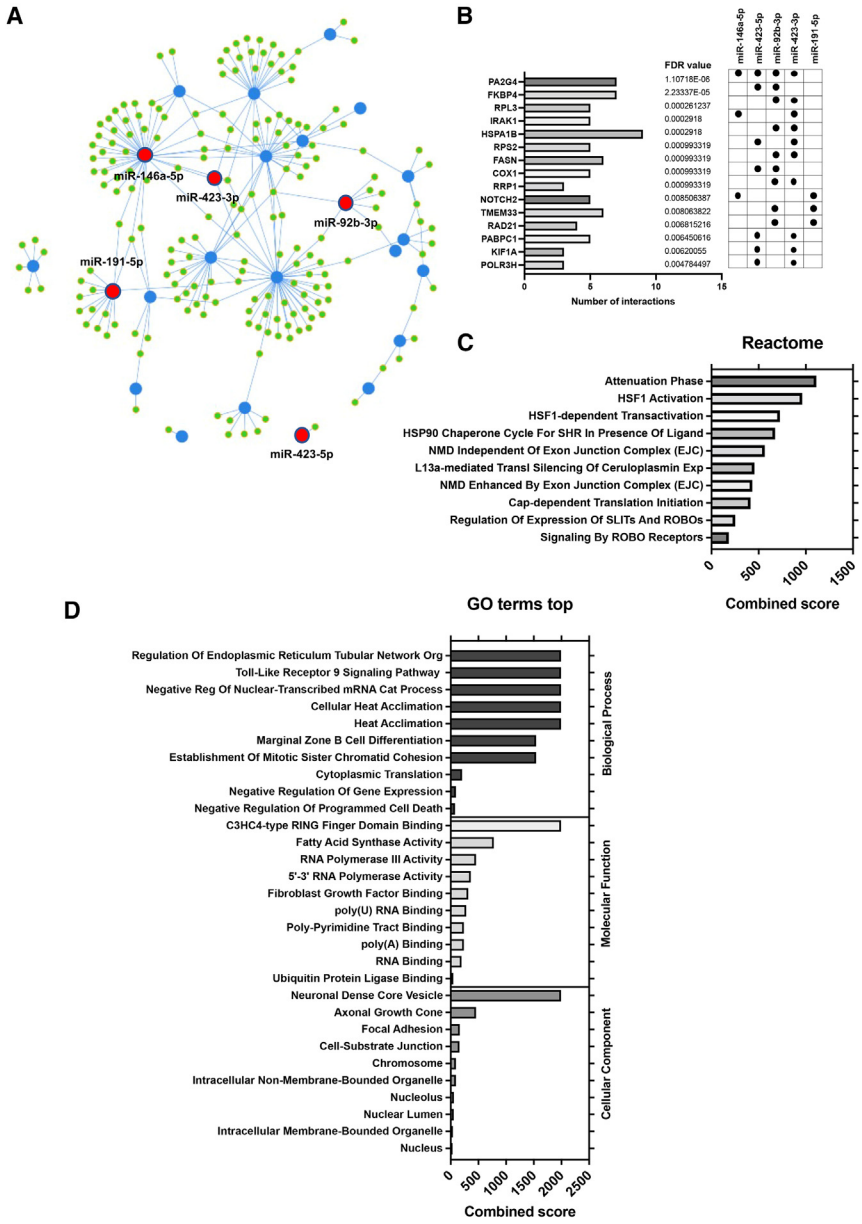


**Figure 3. miRNA-target enrichment analysis of lgEVs and smEVs isolated from WJ-MSCs**

(A) miRNA network as determined by miRTarBase according to minimum number of interactions and p-adjusted (false discovery rate [FDR]) criteria. (B) Predicted targeted genes as sorted by number of interactions (FDR value) and EV-enriched miRNA recognitions. (C) Functional enrichment analyses as performed by Reactome and (D) Go Terms.

decrease in CFP fluorescence after smEV treatment (Figure 4B). Therefore, the dual-reporter assay is a feasible methodology to test the biological target activity of miRNA in EVs. Here, we were able to confirm the target activity of two of the five most enriched miRNAs, miR-92b-3p and miR191-5p in EVs isolated from WJ-MSCs.

### Strategies to increase quantity and immunomodulatory potency of WJ-MSC-derived EVs

It was previously shown that MSCs require an inflammatory challenge to exert potent immunomodulatory effects during inflammation, including the production of immunomodulatory EVs. Therefore, we postulated that pre-conditioning of WJ-MSCs with pro-inflammatory CKs might favor the production and function of both WJ-MSC-derived lgEVs and smEVs. EV fractions were purified from unstimulated or interleukin-1β (IL-1β) and tumor necrosis factor-α (TNF-α)-treated WJ-MSCs (MSC-I/T). The average particle production in lgEVs was similar among WJ-MSCs exposed to IL-1β/TNF-α or control ($1.77 \times 10^9 \pm 3.47 \times 10^8$ vs. $1.69 \times 10^9 \pm 2.86 \times 10^8$, respectively) (Figure 5A). Similarly, we found no significant differences in the number of smEVs produced in CK-treated WJ-MSCs ($1.13 \times 10^{10} \pm 7.53 \times 10^9$) and non-treated controls ($6.32 \times 10^9 \pm 1.04 \times 10^9$). Next, we tested the immunomodulatory potency of lgEVs and smEVs on PHA-activated PBMCs. Of note, lgEVs derived from preconditioned WJ-MSCs displayed enhanced inhibitory effects on activated $CD3^+$ as compared to control (51.3% vs. 30.1%, respectively, $p = 0.0005$) (Figure 5B). Similarly, smEVs derived from CK-treated WJ-MSCs enhanced T cell inhibition (66.7%) as compared to the control group (51.3%, $p = 0.0242$). Thus, inflammatory preconditioning of WJ-MSCs improved the production and anti-inflammatory function of EVs.

Recent evidence pointed to tetraspanin CD9 as a key player in the stability and function of EVs in distinct human cell lines.[35] Here, we tested whether CD9 overexpression in WJ-MSCs would also improve the functional features of lgEVs and smEVs in basal and inflammatory conditions. Constitutive expression of a chimeric construct expressing CD9 linked to GFP ($CD9^{GFP}$) was carried out in WJ-MSCs via lentiviral transduction ($n = 3$ donors). We confirmed the expression of CD9-GFP in LV-transduced WJ-MSCs by flow cytometry (Figure 5C). Interestingly, fluorescence microscopy of subcellular $CD9^{GFP}$ localization revealed that $CD9^{GFP}$ was mainly associated with plasma membranes of WJ-MSCs, without causing alterations in cell morphology (Figure S1E). Remarkably, $CD9^{GFP}$ induced significantly higher levels of EV production as compared to wild-type

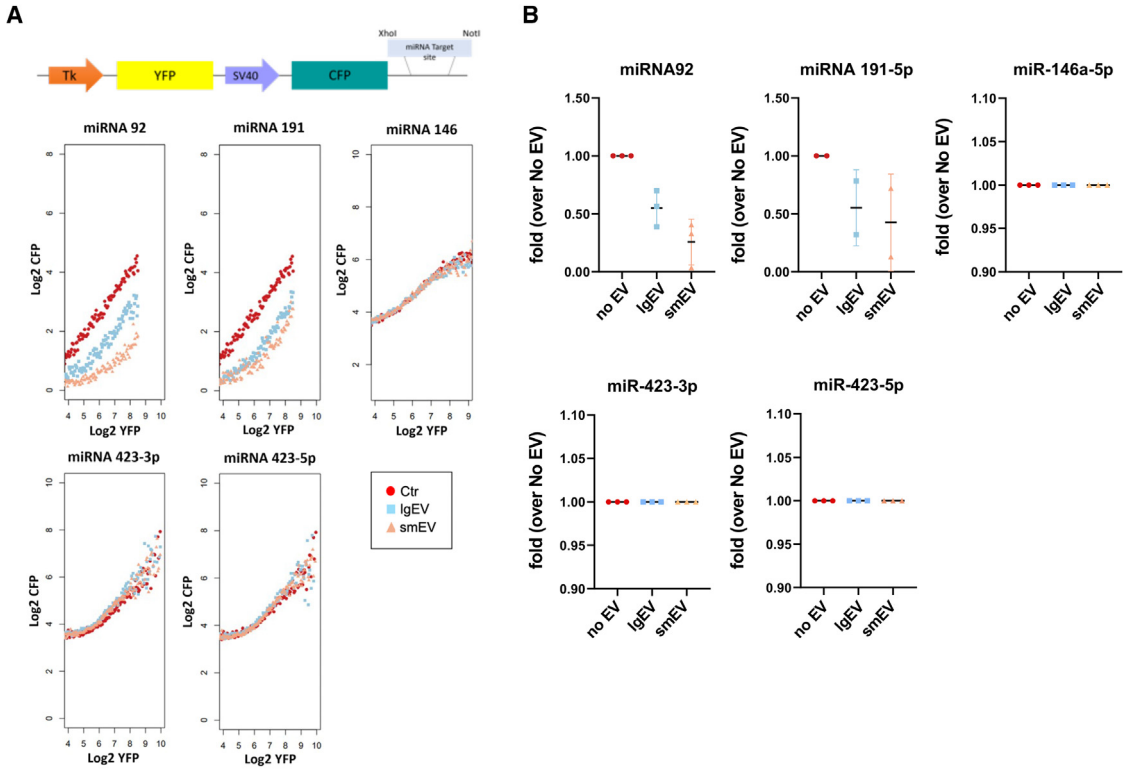


**Figure 4. Functional characterization of miRNA activity by UTA Dual-Fluorescence Reporter System**

(A) Untranslated trans assay (UTA) uses two independent fluorescent proteins expressed individually from two different promoters. CFP contains a complementary target region for tested miRNA adjacent to 3′ UTR and YFP is unaffected. Human HEK293 cells were incubated with lgEVs, smEVs, and medium (no EVs) for 24 h. Subsequently, cells were transfected with five different sensor constructs (miR-146a-5p, miR-423-3p, miR-423-5p, miR-92b-3p, and miR-191-5p) and evaluated after 72 h. Scatterplots for flow cytometry measurements display constant GFP/YFP expression in all the samples within a broad range of fluorescence intensities. (B) Fluorescence intensity ratios of CFP and YFP as compared to no EV control were calculated using custom R scripts. *$p < 0.05$ vs. no EV control.

WJ-MSCs in the smEV fraction ($7.77 \times 10^9 \pm 9.49 \times 10^8$ vs. $1.73 \times 10^{10} \pm 1.06 \times 10^9$ particles, $p = 0.0018$; Figure 5D), which was not associated with the proliferation of WJ-MSCs (Figure S1F). We next investigated a potential synergistic effect of CK preconditioning and $CD9^{GFP}$ overexpression in the immunomodulation of both WJ-MSC-derived lgEVs and smEVs. Both small and large EVs from WJ-MSC-$CD9^{GFP}$ were effective in inhibiting T cell proliferation when compared to PHA-treated PBMCs (Figures 5E and 5F). WJ-MCS-expressing $CD9^{GFP}$ also displayed a potent inhibitory effect in both lgEVs and smEVs isolated from WJ-MSCs. However, the preconditioning of WJ-MSC-$CD9^{GFP}$ with IL-1β and TNF-α did not significantly improve EV-mediated immunomodulation by either lgEVs or smEVs. Finally, we also tested the impact of WJ-MSC EVs on the anti-inflammatory potential of human monocytes/macrophages derived from PBMC donors. Briefly, $CD14^+$ monocytes were magnetically isolated and exposed to lgEVs and smEVs isolated from CK-induced, CD9-expressing or control WJ-MSC for 5 days (approximately 15,000 EVs per cell). Preconditioned monocytes were further co-cultured with activated $CD3^+$ cells (10:1 T cell:monocyte ratio) for an additional 72 h. The proliferation of $CD3^+$ cells was measured, and the inhibition of T cell proliferation was recorded. Non-conditioned or lipopolysaccharide (LPS)-treated monocytes were used as controls. Noticeably, monocytes preconditioned with lgEVs showed superiority in suppressing the proliferation of activated $CD3^+$ cells (approximately 69% vs. 49% in controls, $p < 0.05$) (Figure 5G), regardless of the strategy used in WJ-MSCs. Interestingly, stimulation of CD14 monocytes with smEV preparations derived from CD9-expressing or CK-induced WJ-MSCs exerted a significant suppressive effect on activated T cells (81% and 75%, respectively; $p < 0.01$ vs. control $CD14^+$) (Figure 5H). These data indicate that constitutively, the expression of CD9 or inflammatory preconditioning of WJ-MSC are effective strategies to improve the immunomodulatory function of EV for future immunotherapy applications. Interestingly, these approaches might favor an improved effect of WJ-MSC-derived smEVs in the suppression of activated T cells via monocyte/macrophage immunomodulation.

## DISCUSSION

In this study, we conducted extensive molecular and functional characterization of EVs derived from WJ-MSC. We were able to confirm the purity and uniformity of both lgEV and smEV fractions. Notably, EV fractions exhibited robust immunomodulatory effects in distinct

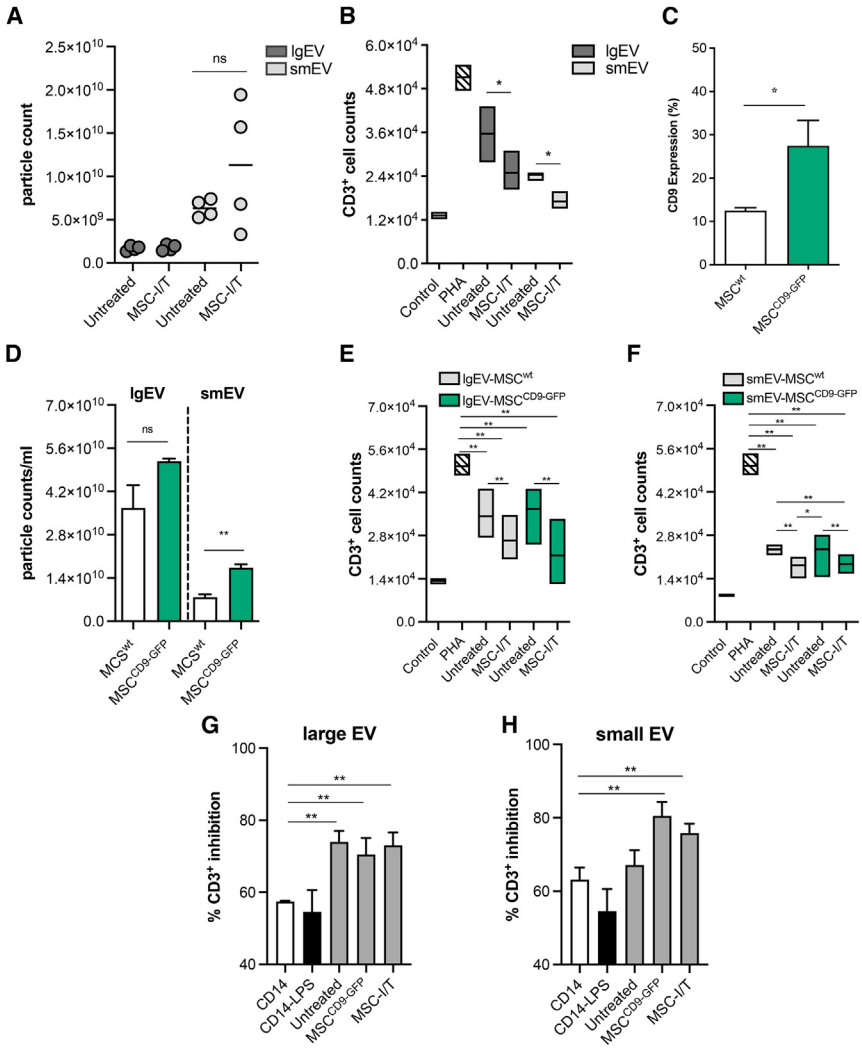


**Figure 5. Characterization of CK preconditioned WJ-MSC-derived EVs**

(A) Absolute EV counts of lgEVs (dark gray dots) and smEVs (light gray dots) derived from preactivated (MSC-I/T) and non-activated (Untreated) WJ-MSC were measured by NTA. Number of particles are displayed as mean from four donors. (B) Inhibitory potential of lgEVs (dark gray boxes) and smEVs (light gray boxes) derived from preactivated (MSC-I/T) and non-activated (Untreated) WJ-MSC on T cell proliferation. PBMCs stimulated with 1 μg/mL PHA were cultured with 4 × $10^3$ lgEV and 1.5 × $10^4$ smEV:PBMCs. After 5 days, T cells were collected and stained with anti-CD3 antibody and cell number was quantified by flow cytometry using CountBright Absolute Counting Beads. (C) Flow cytometry analysis of WJ-MSC constitutively expressing CD9-GFP. (D) Absolute counts of lgEVs and smEVs derived from non-transduced WJ-MSCs ($MSC^{WT}$, white bars) or transduced with LV-CD9-GFP constructs ($MSC^{CD9-GFP}$, green bars). Number of particles are displayed as a media ± SEM (standard error of mean) ($n$ = 4). **$p < 0.01$. (E and F) Inhibitory potential on T cell proliferation of lgEVs and smEVs derived from $MSC^{CD9-GFP}$. PBMCs stimulated with 1 μg/mL PHA were cultured with 4 × $10^3$ lgEVs:PBMCs and 1.5 × $10^4$ smEV:PBMCs isolated after starvation (Untreated) and stimulation with pro-inflammatory CKs (MSC-I/T) for 48 h. After 5 days, T cells were collected and stained with anti-CD3 antibody, and the T cell number was measured by flow cytometry. (G and H) Human $CD14^+$ monocyte/macrophage cells, preconditioned with WJ-MSC-derived lgEVs and smEVs suppress the proliferation of activated T cells. Magnetically separated $CD14^+$ cells from PBMC donors ($n$ = 3) were preconditioned with untreated, CD9-expressing ($MSC^{CD9-GFP}$), or CK-pretreated (MSC-I/T) WJ-MSCs for 5 days. Non-conditioned (CD14) or LPS-treated (CD14-LPS) monocytes were used as controls. Afterward, preconditioned monocytes were co-cultured with activated $CD3^+$ autologous cells for an additional 72 h. $CD3^+$ cell proliferation was recorded and percentage of T cell proliferation inhibition was calculated. Data are represented as mean ± SD of four technical replicas. *$p < 0.05$; **$p < 0.01$. Ctrl, control PBMCs without PHA; lgEV, large extracellular vesicle, PHA, phytohemagglutinin, smEV, small extracellular vesicle.

inflammatory settings, which are associated with the presence of functional miRNAs such as miR-146a-5p, miR-423-3p, miR-423-5p, miR-92b-3p, and miR-191-5p. Furthermore, by applying conditioning strategies on WJ-MSCs such as priming with pro-inflammatory CKs or genetic modifications to enhance CD9 expression, we achieved significant improvements in lgEV and smEV production and potency, consequently elevating their immunomodulatory efficacy *in vitro*. MSCs exert their therapeutic effect via cellular and paracrine processes, leading to the modulation of inflammatory responses at local and systemic levels.[36] MSC-derived EVs have emerged as attractive candidates for cell-free therapeutic applications. Recent progress in the field of EVs has led to ongoing refinement in the isolation and purification methodologies, which in turn has prompted more comprehensive comparative investigations among EV subtypes.[37] Here, we attempted to address fully characterized molecular and functional properties of WJ-MSC-derived lgEVs and smEVs. At present, the purification and enrichment of EVs face technological challenges that could affect product characteristics[38]; for instance, EV cannot be homogeneously purified, but they are partially separated or highly enriched within a given size range.[39–41] Our data indicated successful enrichment of lgEVs by centrifugation at 20,000 × $g$ and smEV at 100,000 × $g$ or PEG precipitation. As for WJ-MSC-lgEVs, isolation using middle-speed centrifugation yielded similar levels of particles in terms of size and quantity, although a small-donor-dependent variability was retained. Regarding WJ-MSC-smEVs, we did not find striking differences between the isolation methods tested, although a greater number of smEVs were isolated using PEG as compared to UC. Interestingly, we confirmed differential expression of CD9 and CD63 in both EV fractions regardless of the isolation method. High heterogeneity has been reported in the expression of macromolecules in EV fractions isolated from different cell types, including bone marrow-derived MSCs (BM-MSCs).[42,43] Of note, other reports were

unable to validate the distinct tetraspanin expression patterns between smEVs and lgEVs.[44,45] Interestingly, CD73, an MSC surface marker, showed greater expression in lgEV fractions, reflecting the identity of WJ-MSC origin, and thus mirroring the cellular source of EVs within our preparation, as was suggested elsewhere.[38,41] We were able to identify two predominant EV subtypes that could be acting as distinct biological entities. Nevertheless, we agree that current isolation protocols may exhibit particular biases toward subsets of EVs or could be permissive for the contamination of non-vesicular particles or protein aggregates,[39] highlighting the absence of a definitive gold standard method for EV purification.

Despite the lack of studies comparing sRNA content between different MSC-derived EVs, their biological activity has been at least in part explained by their miRNA content.[46,47] We observed that fewer than 15% of sRNA species corresponded to miRNAs and demonstrated differential signatures of miRNA expression between cells and their derived EVs. Moreover, we described that a cluster of differential miRNAs were detected in the vesicular fraction, supporting the potential of EVs to transfer specific miRNA species outside the cells. Baglio et al. revealed that primary adipose-derived (AD)-MSC and BM-MSC have sRNA expression profiles dominated by miRNA and small nucleolar RNA (together, 64%–71%). In contrast, the miRNA pool in smEVs was only 2%–5% of the total sRNAome.[17] Other studies showed that miRNA in smEVs do not merely reflect the cellular content and that a defined set of miRNAs are overrepresented in these fractions, as compared to the cell of origin.[17,48] We identified at least 30 differentially expressed miRNAs in WJ-MSC-EVs (Table 1) and demonstrated that lgEV and smEV fractions exhibited similar miRNA expression profiles. Among the top five most enriched miRNAs in WJ-MSC-EVs, we identified that miR-146a-5p, miR-423-3p, miR-423-5p, miR-92b-3p and miR-191-5p have been involved in critical cellular processes linked to immunomodulation and tissue repair. miR-92b-3p together with let-7b-5p and miR-100-5p were recently found in EVs isolated from the neural stem cell line ReNcell and were linked to beneficial effects on the pulmonary hypertension mouse model.[49] Overexpressed miR-92b-3p demonstrated anti-angiogenesis and antitumor effects alone or in combination with apatinib in nude mice abdominal tumor models.[50] miR-191-5p was found to be among the five most abundant miRNAs in AD- and BM-MSC-derived EVs and reported angiogenesis modulation and cell differentiation linked to tissue repair.[17] However, miR-146a-5p is a well-known anti-inflammatory miRNA playing a key role in inflammatory disorders.[51–53] Interestingly, miR-146a was found in smEVs released by dendritic[54] and cardiosphere-derived cells[55] and was transferred between cells to regulate the inflammatory response.[55] Furthermore, Song et al. reported that miR-146a was present in smEVs and transferred to macrophages, where it induced the downregulation of M1 signature and the upregulation of M2 cells. Along with these results, exosomal miR-146a contributed to the increased therapeutic effects of MSCs in an animal model of sepsis.[56] Finally, miR-423 was described as a key player in human hepatic differentiation driven by BM-MSC.[57] By using the UTA-dual-fluorescence reporter system, we were able to demonstrate that highly expressed miR-92b-3p and miR-191-5p were effectively transferred into WJ-MSC-derived EVs and exerted functional regulation in target cells. Thus, this study provides additional evidence of miRNA profiling in WJ-MSC-derived lgEVs and smEVs and demonstrates enrichment or key miRNAs that might be involved in inflammatory and regenerative processes *in vitro* and *in vivo*.

We further demonstrated that WJ-MSC-derived lgEV and smEV-enriched fractions exert potent immunomodulatory response *in vitro* in a dose-dependent manner. Prior extensive research addressed the potential role of EVs in immunomodulation in several models of disease.[10,43,45,58] In general, EVs exerted anti-inflammatory roles via T and B lymphocytes and macrophage modulation. Remarkably, only one study involving human AD-MSC-derived lgEV and smEV fractions revealed anti-inflammatory and chondroprotective effects of EVs, associated with anti-senescence in osteoarthritis chondrocytes *in vitro*.[59–61] Our study demonstrated that lgEV and smEV fractions isolated from human WJ-MSCs triggered similar immunomodulatory potency in *in vitro* models of inflammation. We further aimed to boost the potency of EVs by conditioning EV-producer WJ-MSCs. Based on previous studies, the combination of pro-inflammatory CKs, IL-1β, and TNF-α has not been studied as a strategy to prime WJ-MSCs.[56,62–65] However, a previous systematic study reported that priming MSCs with IL-1β/TNF-α ("early CKs") upregulated IFN-γ receptor expression, which in the context of inflammation enhances their capacity to respond to IFN-γ that is secreted by lymphocytes or natural killer cells arriving at the site of inflammation at a later time point.[66] We observed that WJ-MSC pre-treatment with IL-1β and TNF-α led to a significant increase in the inhibitory effects on T cell proliferation in both lgEVs and smEVs, despite that EV production was similar in conditioned and not-conditioned WJ-MSCs. The inflammatory microenvironment has been shown to induce MSC activation, thereby leading to powerful immunomodulatory responses.[56,67,68] Similar to this study, Ti et al. found that MSCs preactivated with LPS released more Exo containing let7b, which further contributed to improved effects on wound healing.[63] Song et al. demonstrated that IL-1β treatment significantly upregulated miR-146a expression and packaging within exosomes.[56] Only after preactivation with pro-inflammatory CKs did AD-MSC release exosomes with measurable immunosuppressive effects, including M2-like macrophage switch.[69] Contrasting studies showing that MSC priming was not effective in enhancing immunomodulatory effects of EV have also been shown.[70] Cosenza et al. found that IFN-γ priming of MSCs before vesicle isolation did not influence the immunomodulatory function of isolated exosomes or microvesicles.[45] Thus, our results strongly suggest that an inflammatory stimulus may be fundamental to induce the release of immunotherapeutic smEVs and lgEVs from WJ-MSCs. However, due to the high variability of reports regarding immunomodulatory effects of EV, additional research is warranted. This study provides new evidence regarding the pro-inflammatory preconditioning of WJ-MSC as a feasible strategy to improve the lgEV and smEV anti-inflammatory effects on human T cells directly or via monocyte/macrophage condition. Moreover, this study is one of the few reporting a differential

effect *in vitro* for lgEV and smEV isolated from an MSC-human neonatal source primed with pro-inflammatory CKs. Finally, here, we applied a gene engineering strategy to modify WJ-MSCs and evaluate their impact on the production and potency of lgEVs and smEVs. Previously, Böker et al. demonstrated that enhanced expression of the tetraspanin CD9 would result in a significantly increased number of EVs produced in several human cell lines.[35] Later, in a second study, our group[71] used the CD9 expression to boost the exosome output of adeno-associated virus (AAV)-producing HEK-AAV cells. They demonstrated that the yield of exo-AAVs dramatically increased when compared to standard exo-AAVs. Thus, we hypothesize that the genetic engineering of WJ-MSCs to overexpress CD9 might be a feasible molecular strategy to increase EV release and thus improve their immunological potency. Interestingly, here, we demonstrated that CD9-expressing WJ-MSC significantly increased the production of smEVs but not lgEVs without affecting the immunomodulatory potency for both fractions. Remarkably, we found that CD9 transfer together with CK pre-conditioning of WJ-MSC showed improved immunomodulatory effects. Thus, the combination of the two strategies on WJ-MSCs could significantly enhance the development of EV-based cell-free therapies. Further studies should expand on the RNA expression profiles of EV subfractions under inflammation and other experimental conditions, to gain new insights into EV biological processes. Importantly, in the present study, WJ-MSC-derived lgEVs and smEVs did maintain macrophage-polarizing activity that resulted in significantly enhanced anti-proliferative activity of activated T cells. These data suggest that WJ-MSC seem to transfer macrophage-polarizing signals to their EV, which ultimately amplify immunosuppressive activity under inflammatory conditions. Preconditioning or overexpression of CD9 decisively improves this polarizing activity, in particular within the smEV fraction. Finally, this work opens new avenues to explore the effect of WJ-MSC preconditioning and gene transfer strategies on miRNA loading and function in lgEVs and smEVs. More important, additional preclinical research in relevant *in vivo* models of inflammation should close the gap in the role of WJ-MSC-derived EVs in human disease. This research provides new insights into the biology and anti-inflammatory properties of EVs and explores the feasibility of innovative molecular approaches to enhance EV production and potency for future applications.

## MATERIALS AND METHODS

### Isolation and characterization of WJ-MSCs

Human umbilical cords were obtained from healthy donors following vaginal and full-term caesarean with prior informed consent after approval by the ethical committee at Secretaría Distrital de Salud de Bogotá. WJ-MSC were isolated by explant, as previously described.[72] All experiments were performed between passages 2 and 7. WJ-MSCs were characterized by immunophenotyping using the membrane markers CD90 APC (allophycocyanin) (SE10), CD73 PE (phycoerythrin)/Cy7 (AD2), CD105 PE (SN6h), CD45 APC/Cy7 (2D1), CD34 PerCP/Cy5.5 (561), HLA-DR Pacific Blue (L243), and HLA-ABC FITC (fluorescein isothiocyanate) (W6/32) or corresponding isotype controls (all from BioLegend, USA) and analyzed by flow cytometry (BD FACSCanto II, USA). Multilineage potential was confirmed by inducing specific lineage commitment (osteogenic, chondrogenic, and adipogenic differentiation), as previously described.[72]

### EV production from WJ-MSC cultures

For EV production, WJ-MSC cultures at 70% confluence were treated under two conditions: serum deprivation (starvation) and pro-inflammation. Inflammatory stimuli consisted of DMEM supplemented with recombinant human TNF-α and IL-1β, 10 ng/mL each (BioLegend). Following 48 h of treatment, CM was collected and lgEV and smEV fractions were isolated. For WJ-MSC-lgEV enrichment, CMs were centrifuged at 2,000 × *g* for 10 min, followed by centrifugation at 20,000 × *g*, 30 or 60 min at 4°C. The resulting pellet was either resuspended in double-filtered PBS or RPMI medium. MSC-smEV were further enriched using two methodologies: UC and PEG precipitation. Accordingly, CM resulting from WJ-MSC-lgEV isolation was passed through 0.22-μm filters and ultracentrifuged at 100,000 × *g* for 90 min at 4°C. The smEV pellet was further re-suspended in double-filtered PBS or RPMI medium. For PEG precipitation, 0.22-μm filtered CM resulting from lgEV isolation was mixed in a 1:5 ratio with PEG solution (PEG8000 in PBS at 500 mg/mL) and incubated at 4°C. After 16 h, the samples were centrifuged at 1,500 × *g* for 30 min at 4°C. smEVs were re-suspended in double-filtered PBS or RPMI medium.

### NTA of WJ-MSC-EV

Isolated WJ-MSC-EVs were characterized based on their particle size and concentration using nanoparticle tracking analysis (NTA). Briefly, WJ-MS lgEVs and smEVs were diluted at 1:10 to 1:100 with sterile-filtered PBS and analyzed using the NanoSight NS300 instrument (Malvern Panalytical, UK), following the manufacturer's protocol. Samples were recorded in triplicate for 30 s. The data were processed using NTA software version 2.3 (Malvern Panalytical).

### Immunoblotting of WJ-MSC-EVs

For western blot analysis, EV samples were analyzed with the following antibodies, all at a 1:1,000 dilution: anti-CD81 (clone M38; catalog no. 10630D, Invitrogen, USA), anti-Alix (EP23653-32; catalog no. ab275377, Abcam, UK), and anti-ApoAI (EP1368Y; catalog no. ab52945, Abcam, UK). Briefly, EV samples in PBS were prepared with 6× sample buffer with (reducing) or without (non-reducing) 50 mM DTT to a final 1× concentration and heated at 70°C for 10 min. Samples were then subjected to SDS-PAGE and followed by transfer to a polyvinylidene fluoride (PVDF) membrane (catalog no. 88518, Thermo Fisher Scientific, USA). PVDF membranes were blocked and incubated with primary antibodies in 1% milk overnight at 4°C. Washed membrane was probed with horseradish peroxidase-conjugated secondary antibodies at a 1:10,000 dilution. Signals were developed using the Pierce ECL Western Blotting Substrate (catalog no. 32106, Thermo Fisher Scientific) and imaged using a Vilber Fusion Fx Spectra imaging system.

### Membrane marker characterization of WJ-MSC-EV by flow cytometry

Expression of tetraspanins CD9, CD81, and CD63 and the WJ-MSC marker CD73 were assessed on the EV surface by an indirect method

based on flow cytometry. Briefly 10 μL (1:100 dilution) of 4-μm aldehyde/sulfate latex beads (Life Technologies, USA) were mixed with EV suspension in 800:1 (lgEV) or 1,600:1 (smEV) ratio per bead in PBS. The mix was further incubated on a rotary wheel for 1 h at room temperature (RT). WJ-MSC-EV-bead complexes were centrifuged and blocked with BSA 7.5% (BSA Fraction V, 7.5%, Gibco, USA) for 30 min at RT and further incubated with CD63-FITC (H5C6), CD9-PE (HI9a) and CD81 (TAPA-1)-APC (5A6) antibodies or corresponding isotype controls (BioLegend) for an additional 30 min at 4°C. Following centrifugation, pellets with lgEV and smEV beads were re-suspended in sterile-filtered PBS acquired in a BD LSR II system and analyzed with FlowJo software (Tree Star, USA).

### Generation of $CD9^{GFP}$-expressing WJ-MSCs

The $CD9^{GFP}$ fusion protein was cloned as previously described[35] from Emerald-CD9-10 (Addgene plasmid no. 54029, a gift from Michael Davidson) into the pENTR1a no CCDB. Gateway cloning with Lambda recombination reaction was performed according to the manufacturer's protocol using second-generation lentiviral vectors pLENTI6.3/TO/V5-Dest (Thermo Fisher Scientific). $CD9^{GFP}$ pseudotyped lentiviruses were produced in HEK293FT cells. Cells were seeded in two T75 flasks at $8.25 \times 10^5$ cells/mL and directly transfected with pLenti-$CD9^{GFP}$, viral capsid plasmid psPAX2 (Addgene plasmid no. 12260, a gift from Didier Trono), and pseudotype pCMV-VSV-G envelope plasmid (Addgene plasmid no. 8454, a gift from Bob Weinberg).[73] After 16 h of transfection, sodium butyrate-containing media (10 mM) was added for 8 h. Supernatants containing viral particles were collected after 5 days, centrifuged for 30 min at $2{,}000 \times g$, filtered (0.45 μm), and stored at −80°C. WJ-MSC cells were seeded in a 24-well plate (100,000 cells/well) and transduced for 72 h. Constitutive expression of $CD9^{GFP}$ was confirmed by fluorescence microscopy (Axio Observer microscope, Zeiss, Germany). Transduction efficiency was determined by quantifying GFP-expressing cells using the BD LSR II flow cytometry system (BD, USA) and analyzed with FlowJo software. EVs produced from $CD9^{GFP}$-expressing WJ-MSC were isolated and characterized as previously described.

### T cell proliferation assay

The immunomodulatory effect of WJ-MSC-EV was evaluated in T cell proliferation immunoassays. PBMCs were obtained from healthy donors by gradient centrifugation using Lymphoprep (Abbott, USA). After 24 h in culture, $1 \times 10^5$ PBMCs were seeded in 96-well flat-bottomed plates, stimulated with 1 μg/mL PHA or anti-CD2, -CD3, -CD28 T cell activation beads (Miltenyi Biotec, Germany) and exposed to different ratios of WJ-MSC-lgEVs ($1:1 \times 10^3$ to $1:4 \times 10^3$) or WJ-MSC-smEV ($1:5 \times 10^3$ to $1: 1.5 \times 10^4$) in a total volume of 150 μL/well. Unstimulated PBMCs were used as basal control. Experiments were also performed with EVs obtained from WJ-MSCs preconditioned with pro-inflammatory CKs and WJ-MSCs expressing $CD9^{GFP}$. T cell cultures (triplicate) were incubated for 5 days. In a different set of experiments, $CD14^+$ monocytes derived from PBMC donors ($n = 2$–3) were magnetically separated (Miltenyi Biotec) and exposed to lgEV and smEV fractions in a ratio of 15,000/cell, for 5 days. EV-conditioned monocytes were further occulted with autologous PBMCs (10 PBMCs to 1 conditioned monocyte) for an additional 72 h. The effect of WJ-MSC-EVs of EV-conditioned monocytes on T cell proliferation was measured by $CD3^+$ absolute counts (CD3 PE/Cy7, HIT3a, BioLegend) using CountBright Absolute Counting Beads and flow cytometry (Life Technologies). The number of cells per microliter was calculated with the number of counted cells × concentration of beads/number of counted beads.

### RNA isolation and sRNA sequencing by NGS

Total RNA from WJ-MSC lgEVs and smEV and EV-producer WJ-MSCs was isolated via phenol/chloroform extraction (Trizol, Thermo Fisher Scientific). RNA was measured by the Synergy system (BioTek, USA); 1,000 ng of total RNA was reverse transcribed using Sensifast cDNA Synthesis Kit (Bioline, UK) and diluted (1:5 or 1:10). Furthermore, RNA was measured on the BioAnalyzer system (Agilent, USA) via the RNA 6000 Pico Kit (Agilent), and the RNA amount, size distribution, and RNA integrity number was analyzed.

### UTA

HEK293 FT cells were cultured in DMEM High Glucose supplemented with 5% FBS at 37°C with 5% $CO_2$. To generate the reporter plasmids with the miRNA response element, the constructs were cloned according to Lemus-Diaz et al.[74] Shortly after, sRNA sequences were derived from miRBase (www.mirbase.org), and oligonucleotides (Table S1) were designed with NotI and XhoI overhangs. Oligonucleotides were annealed and ligated into the plasmid p.UTA.2.0 (catalog no. 82446, Addgene) using NotI and XhoI restriction enzymes. To check for the correct oligonucleotide insertion, we performed endonuclease restriction and sequencing. Subsequently p.UTA.2.0 plasmids were transfected. In 24-well plates, $4 \times 10^4$ HEK297 cells/well were seeded and cultured for 24 h under the conditions described. Next, the medium was discarded and replaced with 100 μL DMEM High Glucose supplemented with 200 μL WJ-MSC-derived EVs, and the cells were incubated for an additional 24 h. DNA plasmid (p.UTA.2.0, 5 μg, per each construct, transfected in independent assays) was transfected with Lipofectamine 2000 (Thermo Fisher) and incubated for 24 h at 37°C and 5% $CO_2$. Afterward, transfection medium was replaced with 100 μL DMEM High Glucose supplemented with 200 μL WJ-MSC-derived EVs, and the cells were incubated for an additional 24 h. Finally, cells were trypsinized and prepared for flow cytometry. Flow cytometry was performed on a BD FACSCanto II instrument. Flow cytometry standard files were exported and analyzed on R using the methodology employed in Lemus-Diaz et al.[74]

### Bioinformatic and statistical analyses

Sequence data from FASTQ files were processed, aligned to sRNA databases, and the reads were subsequently normalized. For the detection of differentially expressed miRNA, edgeR, DESeq, and NOISeq methods were applied. Sample quality and sequencing reproducibility were ensured by using heatmaps and blind hierarchal clustering. MIENTURNET was used for experimentally validated miRNA target interactions from TargetScan and miRTarBase. To determine

statistical significances, we used Student's t and ANOVA tests for parametric data and the Kruskal-Wallis test for non-parametric data. The level of significance was considered when the $p$ value was below 0.05. Statistical analysis was carried out using GraphPad Prism version 8.0.1 software (GraphPad, USA).

## DATA AND CODE AVAILABILITY

Data supporting the findings of this work are available within the paper and the supplemental information files.

## ACKNOWLEDGMENTS

J.C.B. received a Ph.D. scholarship from Universidad del Rosario. This research was funded by grants from the Colombian Ministry of Science, Technology, and Innovation and the German Ministry of Science and Education BPIN2016000100035 and FP44842-157-2017.

## AUTHOR CONTRIBUTIONS

G.S. and J.G. conceived the project. J.C.B. and M.C.-B. performed most experiments and analyzed the primary data. J.C.B. wrote the manuscript. V.D.-A. performed the dual-fluorescence experiments and analyzed the primary data. C.M. and N.F. performed the bioinformatic analysis. G.S. and J.G. provided permanent direction during the experiments, data analysis, and manuscript preparation.

## DECLARATION OF INTERESTS

The authors declare no competing interests.

## SUPPLEMENTAL INFORMATION

Supplemental information can be found online at https://doi.org/10.1016/j.omtm.2024.101353.

## REFERENCES

1. Colter, D.C., Class, R., DiGirolamo, C.M., and Prockop, D.J. (2000). Rapid expansion of recycling stem cells in cultures of plastic-adherent cells from human bone marrow. Proc. Natl. Acad. Sci. USA *97*, 3213–3218. https://doi.org/10.1073/pnas.070034097.

2. Zuk, P.A., Zhu, M., Ashjian, P., De Ugarte, D.A., Huang, J.I., Mizuno, H., Alfonso, Z.C., Fraser, J.K., Benhaim, P., and Hedrick, M.H. (2002). Human adipose tissue is a source of multipotent stem cells. Mol. Biol. Cell *13*, 4279–4295. https://doi.org/10.1091/mbc.e02-02-0105.

3. Miranda Rodríguez, A., Galván Cabrera, J.A., and de León Delgado, J. (2015). Propiedades inmunomoduladoras de las células madre mesenquimales. Rev. Cubana Hematol. Inmunol. Hemoter. *31*, 20–31. http://scielo.sld.cu/scielo.php?script=sci_arttext&pid=S0864-02892015000100003&nrm=iso.

4. Raposo, G., and Stoorvogel, W. (2013). Extracellular vesicles: exosomes, microvesicles, and friends. J. Cell Biol. *200*, 373–383. https://doi.org/10.1083/jcb.201211138.

5. Kalra, H., Simpson, R.J., Ji, H., Aikawa, E., Altevogt, P., Askenase, P., Bond, V.C., Borràs, F.E., Breakefield, X., Budnik, V., et al. (2012). Vesiclepedia: a compendium for extracellular vesicles with continuous community annotation. PLoS Biol. *10*, e1001450. https://doi.org/10.1371/journal.pbio.1001450.

6. Tofiño-Vian, M., Guillen, M.I., and Alcaraz, M.J. (2018). Extracellular vesicles: A new therapeutic strategy for joint conditions. Biochem. Pharmacol. *153*, 134–146. https://doi.org/10.1016/j.bcp.2018.02.004.

7. Akers, J.C., Gonda, D., Kim, R., Carter, B.S., and Chen, C.C. (2013). Biogenesis of extracellular vesicles (EV): exosomes, microvesicles, retrovirus-like vesicles, and apoptotic bodies. J. Neuro Oncol. *113*, 1–11. https://doi.org/10.1007/s11060-013-1084-8.

8. Gyorgy, B., Szabo, T.G., Turiak, L., Wright, M., Herczeg, P., Ledeczi, Z., Kittel, A., Polgar, A., Toth, K., Derfalvi, B., et al. (2012). Improved flow cytometric assessment reveals distinct microvesicle (cell-derived microparticle) signatures in joint diseases. PLoS One *7*, e49726. https://doi.org/10.1371/journal.pone.0049726.

9. Nawaz, M., Fatima, F., Vallabhaneni, K.C., Penfornis, P., Valadi, H., Ekström, K., Kholia, S., Whitt, J.D., Fernandes, J.D., Pochampally, R., et al. (2016). Extracellular Vesicles: Evolving Factors in Stem Cell Biology. Stem Cells Int. *2016*, 1073140. https://doi.org/10.1155/2016/1073140.

10. Wen, S., Dooner, M., Cheng, Y., Papa, E., Del Tatto, M., Pereira, M., Deng, Y., Goldberg, L., Aliotta, J., Chatterjee, D., et al. (2016). Mesenchymal stromal cell-derived extracellular vesicles rescue radiation damage to murine marrow hematopoietic cells. Leukemia *30*, 2221–2231. https://doi.org/10.1038/leu.2016.107.

11. de Godoy, M.A., Saraiva, L.M., de Carvalho, L.R.P., Vasconcelos-Dos-Santos, A., Beiral, H.J.V., Ramos, A.B., Silva, L.R.P., Leal, R.B., Monteiro, V.H.S., Braga, C.V., et al. (2018). Mesenchymal stem cells and cell-derived extracellular vesicles protect hippocampal neurons from oxidative stress and synapse damage induced by amyloid-beta oligomers. J. Biol. Chem. *293*, 1957–1975. https://doi.org/10.1074/jbc.M117.807180.

12. Asgarpour, K., Shojaei, Z., Amiri, F., Ai, J., Mahjoubin-Tehran, M., Ghasemi, F., Arefnezhad, R., Hamblin, M.R., and Mirzaei, H. (2020). Exosomal microRNAs derived from mesenchymal stem cells: cell-to-cell messages. Cell Commun. Signal. *18*, 149. https://doi.org/10.1186/s12964-020-00650-6.

13. Groot, M., and Lee, H. (2020). Sorting Mechanisms for MicroRNAs into Extracellular Vesicles and Their Associated Diseases. Cells *9*, 1044. https://doi.org/10.3390/cells9041044.

14. Rappa, G., Santos, M.F., Green, T.M., Karbanová, J., Hassler, J., Bai, Y., Barsky, S.H., Corbeil, D., and Lorico, A. (2017). Nuclear transport of cancer extracellular vesicle-derived biomaterials through nuclear envelope invagination-associated late endosomes. Oncotarget *8*, 14443–14461. https://doi.org/10.18632/oncotarget.14804.

15. Santos, M.F., Rappa, G., Karbanová, J., Vanier, C., Morimoto, C., Corbeil, D., and Lorico, A. (2019). Anti-human CD9 antibody Fab fragment impairs the internalization of extracellular vesicles and the nuclear transfer of their cargo proteins. J. Cell Mol. Med. *23*, 4408–4421. https://doi.org/10.1111/jcmm.14334.

16. Nigri, J., Leca, J., Tubiana, S.S., Finetti, P., Guillaumond, F., Martinez, S., Lac, S., Iovanna, J.L., Audebert, S., Camoin, L., et al. (2022). CD9 mediates the uptake of extracellular vesicles from cancer-associated fibroblasts that promote pancreatic cancer cell aggressiveness. Sci. Signal. *15*, eabg8191. https://doi.org/10.1126/scisignal.abg8191.

17. Baglio, S.R., Rooijers, K., Koppers-Lalic, D., Verweij, F.J., Pérez Lanzón, M., Zini, N., Naaijkens, B., Perut, F., Niessen, H.W.M., Baldini, N., and Pegtel, D.M. (2015). Human bone marrow- and adipose-mesenchymal stem cells secrete exosomes enriched in distinctive miRNA and tRNA species. Stem Cell Res. Ther. *6*, 127. https://doi.org/10.1186/s13287-015-0116-z.

18. Skog, J., Würdinger, T., Van Rijn, S., Meijer, D.H., Gainche, L., Sena-Esteves, M., Curry, W.T., Jr., Carter, B.S., Krichevsky, A.M., and Breakefield, X.O. (2008). Glioblastoma microvesicles transport RNA and proteins that promote tumour growth and provide diagnostic biomarkers. Nat. Cell Biol. *10*, 1470–1476. https://doi.org/10.1038/ncb1800.

19. Valadi, H., Ekström, K., Bossios, A., Sjöstrand, M., Lee, J.J., and Lötvall, J.O. (2007). Exosome-mediated transfer of mRNAs and microRNAs is a novel mechanism of genetic exchange between cells. Nat. Cell Biol. *9*, 654–659. https://doi.org/10.1038/ncb1596.

20. Nolte-'T Hoen, E.N.M., Buermans, H.P.J., Waasdorp, M., Stoorvogel, W., Wauben, M.H.M., and 't Hoen, P.A.C. (2012). Deep sequencing of RNA from immune cell-derived vesicles uncovers the selective incorporation of small non-coding RNA biotypes with potential regulatory functions. Nucleic Acids Res. *40*, 9272–9285. https://doi.org/10.1093/nar/gks658.

21. Xie, X., Ji, J., Chen, X., Xu, W., Chen, H., Zhu, S., Wu, J., Wu, Y., Sun, Y., Sai, W., et al. (2022). Human umbilical cord mesenchymal stem cell-derived exosomes carrying hsa-miRNA-128-3p suppress pancreatic ductal cell carcinoma by inhibiting Galectin-3. Clin. Transl. Oncol. *24*, 517–531. https://doi.org/10.1007/s12094-021-02705-7.

22. Fang, S., Xu, C., Zhang, Y., Xue, C., Yang, C., Bi, H., Qian, X., Wu, M., Ji, K., Zhao, Y., et al. (2016). Umbilical Cord-Derived Mesenchymal Stem Cell-Derived Exosomal MicroRNAs Suppress Myofibroblast Differentiation by Inhibiting the Transforming Growth Factor-β/SMAD2 Pathway During Wound Healing. Stem Cells Transl. Med. *5*, 1425–1439. https://doi.org/10.5966/sctm.2015-0367.

23. Yang, M., Liu, X., Jiang, M., Li, J., Tang, Y., and Zhou, L. (2021). miR-543 in human mesenchymal stem cell-derived exosomes promotes cardiac microvascular

endothelial cell angiogenesis after myocardial infarction through COL4A1. IUBMB Life *73*, 927–940. https://doi.org/10.1002/iub.2474.

24. Avendaño-Félix, M., Fuentes-Mera, L., Ramos-Payan, R., Aguilar-Medina, M., Pérez-Silos, V., Moncada-Saucedo, N., Marchat, L.A., González-Barrios, J.A., Ruiz-García, E., Astudillo-de la Vega, H., et al. (2019). A Novel OsteomiRs Expression Signature for Osteoblast Differentiation of Human Amniotic Membrane-Derived Mesenchymal Stem Cells. BioMed Res. Int. *2019*, 8987268. https://doi.org/10.1155/2019/8987268.

25. Li, J., Hu, C., Han, L., Liu, L., Jing, W., Tang, W., Tian, W., and Long, J. (2015). MiR-154-5p regulates osteogenic differentiation of adipose-derived mesenchymal stem cells under tensile stress through the Wnt/PCP pathway by targeting Wnt11. Bone *78*, 130–141. https://doi.org/10.1016/j.bone.2015.05.003.

26. Gu, W., Hong, X., Le Bras, A., Nowak, W.N., Issa Bhaloo, S., Deng, J., Xie, Y., Hu, Y., Ruan, X.Z., and Xu, Q. (2018). Smooth muscle cells differentiated from mesenchymal stem cells are regulated by microRNAs and suitable for vascular tissue grafts. J. Biol. Chem. *293*, 8089–8102. https://doi.org/10.1074/jbc.RA118.001739.

27. Tang, Q., Lu, B., He, J., Chen, X., Fu, Q., Han, H., Luo, C., Yin, H., Qin, Z., Lyu, D., et al. (2022). Exosomes-loaded thermosensitive hydrogels for corneal epithelium and stroma regeneration. Biomaterials *280*, 121320. https://doi.org/10.1016/j.biomaterials.2021.121320.

28. Wu, L., Zhang, G., Guo, C., Zhao, X., Shen, D., and Yang, N. (2020). MiR-128-3p mediates TNF-α-induced inflammatory responses by regulating Sirt1 expression in bone marrow mesenchymal stem cells. Biochem. Biophys. Res. Commun. *521*, 98–105. https://doi.org/10.1016/j.bbrc.2019.10.083.

29. Weilner, S., Skalicky, S., Salzer, B., Keider, V., Wagner, M., Hildner, F., Gabriel, C., Dovjak, P., Pietschmann, P., Grillari-Voglauer, R., et al. (2015). Differentially circulating miRNAs after recent osteoporotic fractures can influence osteogenic differentiation. Bone *79*, 43–51. https://doi.org/10.1016/j.bone.2015.05.027.

30. Khosravi, M., Azarpira, N., Shamdani, S., Hojjat-Assari, S., Naserian, S., and Karimi, M.H. (2018). Differentiation of umbilical cord derived mesenchymal stem cells to hepatocyte cells by transfection of miR-106a, miR-574-3p, and miR-451. Gene *667*, 1–9. https://doi.org/10.1016/j.gene.2018.05.028.

31. Guérit, D., Philipot, D., Chuchana, P., Toupet, K., Brondello, J.-M., Mathieu, M., Jorgensen, C., and Noël, D. (2013). Sox9-Regulated miRNA-574-3p Inhibits Chondrogenic Differentiation of Mesenchymal Stem Cells. PLoS One *8*, e62582. https://doi.org/10.1371/journal.pone.0062582.

32. Peltzer, J., Lund, K., Goriot, M.E., Grosbot, M., Lataillade, J.J., Mauduit, P., and Banzet, S. (2020). Interferon-γ and Hypoxia Priming Have Limited Effect on the miRNA Landscape of Human Mesenchymal Stromal Cells-Derived Extracellular Vesicles. Front. Cell Dev. Biol. *8*, 581436. https://doi.org/10.3389/fcell.2020.581436.

33. Li, K., Yan, G., Huang, H., Zheng, M., Ma, K., Cui, X., Lu, D., Zheng, L., Zhu, B., Cheng, J., and Zhao, J. (2022). Anti-inflammatory and immunomodulatory effects of the extracellular vesicles derived from human umbilical cord mesenchymal stem cells on osteoarthritis via M2 macrophages. J. Nanobiotechnol. *20*, 38. https://doi.org/10.1186/s12951-021-01236-1.

34. Lemus-Diaz, N., Böker, K.O., Rodriguez Polo, I., Mitter, M., Preis, J., Arlt, M., and Gruber, J. (2017). Dissecting miRNA gene repression on single cell level with an advanced fluorescent reporter system. Sci. Rep. *7*, 45197. https://doi.org/10.1038/srep45197.

35. Böker, K.O., Lemus-Diaz, N., Rinaldi Ferreira, R., Schiller, L., Schneider, S., and Gruber, J. (2018). The Impact of the CD9 Tetraspanin on Lentivirus Infectivity and Exosome Secretion. Mol. Ther. *26*, 634–647. https://doi.org/10.1016/j.ymthe.2017.11.008.

36. Mathieu, M., Martin-Jaular, L., Lavieu, G., and Théry, C. (2019). Specificities of secretion and uptake of exosomes and other extracellular vesicles for cell-to-cell communication. Nat. Cell Biol. *21*, 9–17. https://doi.org/10.1038/s41556-018-0250-9.

37. Merchant, M.L., Rood, I.M., Deegens, J.K.J., and Klein, J.B. (2017). Isolation and characterization of urinary extracellular vesicles: implications for biomarker discovery. Nat. Rev. Nephrol. *13*, 731–749. https://doi.org/10.1038/nrneph.2017.148.

38. Gimona, M., Brizzi, M.F., Choo, A.B.H., Dominici, M., Davidson, S.M., Grillari, J., Hermann, D.M., Hill, A.F., De Kleijn, D., Lai, R.C., et al. (2021). Critical considerations for the development of potency tests for therapeutic applications of mesenchymal stromal cell-derived small extracellular vesicles. Cytotherapy *23*, 373–380. https://doi.org/10.1016/j.jcyt.2021.01.001.

39. Monguió-Tortajada, M., Gálvez-Montón, C., Bayes-Genis, A., Roura, S., and Borràs, F.E. (2019). Extracellular vesicle isolation methods: rising impact of size-exclusion chromatography. Cell. Mol. Life Sci. *76*, 2369–2382. https://doi.org/10.1007/s00018-019-03071-y.

40. Reiner, A.T., Witwer, K.W., Van Balkom, B.W.M., De Beer, J., Brodie, C., Corteling, R.L., Gabrielsson, S., Gimona, M., Ibrahim, A.G., De Kleijn, D., et al. (2017). Concise Review: Developing Best-Practice Models for the Therapeutic Use of Extracellular Vesicles. Stem Cells Transl. Med. *6*, 1730–1739. https://doi.org/10.1002/sctm.17-0055.

41. Witwer, K.W., Van Balkom, B.W.M., Bruno, S., Choo, A., Dominici, M., Gimona, M., Hill, A.F., De Kleijn, D., Koh, M., Lai, R.C., et al. (2019). Defining mesenchymal stromal cell (MSC)-derived small extracellular vesicles for therapeutic applications. J. Extracell. Vesicles *8*, 1609206. https://doi.org/10.1080/20013078.2019.1609206.

42. Lai, R.C., Tan, S.S., Yeo, R.W.Y., Choo, A.B.H., Reiner, A.T., Su, Y., Shen, Y., Fu, Z., Alexander, L., Sze, S.K., and Lim, S.K. (2016). MSC secretes at least 3 EV types each with a unique permutation of membrane lipid, protein and RNA. J. Extracell. Vesicles *5*, 29828. https://doi.org/10.3402/jev.v5.29828.

43. Collino, F., Pomatto, M., Bruno, S., Lindoso, R.S., Tapparo, M., Sicheng, W., Quesenberry, P., and Camussi, G. (2017). Exosome and Microvesicle-Enriched Fractions Isolated from Mesenchymal Stem Cells by Gradient Separation Showed Different Molecular Signatures and Functions on Renal Tubular Epithelial Cells. Stem Cell Rev. Rep. *13*, 226–243. https://doi.org/10.1007/s12015-016-9713-1.

44. Cosenza, S., Ruiz, M., Toupet, K., Jorgensen, C., and Noël, D. (2017). Mesenchymal stem cells derived exosomes and microparticles protect cartilage and bone from degradation in osteoarthritis. Sci. Rep. *7*, 16214. https://doi.org/10.1038/s41598-017-15376-8.

45. Cosenza, S., Toupet, K., Maumus, M., Luz-Crawford, P., Blanc-Brude, O., Jorgensen, C., and Noël, D. (2018). Mesenchymal stem cells-derived exosomes are more immunosuppressive than microparticles in inflammatory arthritis. Theranostics *8*, 1399–1410. https://doi.org/10.7150/thno.21072.

46. Momen-Heravi, F., Bala, S., Kodys, K., and Szabo, G. (2015). Exosomes derived from alcohol-treated hepatocytes horizontally transfer liver specific miRNA-122 and sensitize monocytes to LPS. Sci. Rep. *5*, 9991. https://doi.org/10.1038/srep09991.

47. Lindoso, R.S., Collino, F., Bruno, S., Araujo, D.S., Sant'Anna, J.F., Tetta, C., Provero, P., Quesenberry, P.J., Vieyra, A., Einicker-Lamas, M., and Camussi, G. (2014). Extracellular Vesicles Released from Mesenchymal Stromal Cells Modulate miRNA in Renal Tubular Cells and Inhibit ATP Depletion Injury. Stem Cell. Dev. *23*, 1809–1819. https://doi.org/10.1089/scd.2013.0618.

48. Ji, H., Chen, M., Greening, D.W., He, W., Rai, A., Zhang, W., and Simpson, R.J. (2014). Deep Sequencing of RNA from Three Different Extracellular Vesicle (EV) Subtypes Released from the Human LIM1863 Colon Cancer Cell Line Uncovers Distinct Mirna-Enrichment Signatures. PLoS One *9*, e110314. https://doi.org/10.1371/journal.pone.0110314.

49. Wang, J., Hu, L., Huang, H., Yu, Y., Wang, J., Yu, Y., Li, K., Li, Y., Tian, T., and Chen, F. (2020). CAR (CARSKNKDC) Peptide Modified ReNcell-Derived Extracellular Vesicles as a Novel Therapeutic Agent for Targeted Pulmonary Hypertension Therapy. Hypertension *76*, 1147–1160. https://doi.org/10.1161/HYPERTENSIONAHA.120.15554.

50. Wang, J., Wang, C., Li, Y., Li, M., Zhu, T., Shen, Z., Wang, H., Lv, W., Wang, X., Cheng, X., and Xie, X. (2021). Potential of peptide-engineered exosomes with overexpressed miR-92b-3p in anti-angiogenic therapy of ovarian cancer. Clin. Transl. Med. *11*, e425. https://doi.org/10.1002/ctm2.425.

51. Boldin, M.P., Taganov, K.D., Rao, D.S., Yang, L., Zhao, J.L., Kalwani, M., Garcia-Flores, Y., Luong, M., Devrekanli, A., Xu, J., et al. (2011). miR-146a is a significant brake on autoimmunity, myeloproliferation, and cancer in mice. J. Exp. Med. *208*, 1189–1201. https://doi.org/10.1084/jem.20101823.

52. Williams, A.E., Perry, M.M., Moschos, S.A., Larner-Svensson, H.M., and Lindsay, M.A. (2008). Role of miRNA-146a in the regulation of the innate immune response and cancer. Biochem. Soc. Trans. *36*, 1211–1215. https://doi.org/10.1042/BST0361211.

53. Taganov, K.D., Boldin, M.P., Chang, K.J., and Baltimore, D. (2006). NF-kappaB-dependent induction of microRNA miR-146, an inhibitor targeted to signaling proteins of innate immune responses. Proc. Natl. Acad. Sci. USA *103*, 12481–12486. https://doi.org/10.1073/pnas.0605298103.

54. Alexander, M., Hu, R., Runtsch, M.C., Kagele, D.A., Mosbruger, T.L., Tolmachova, T., Seabra, M.C., Round, J.L., Ward, D.M., and O'Connell, R.M. (2015). Exosome-delivered microRNAs modulate the inflammatory response to endotoxin. Nat. Commun. *6*, 7321. https://doi.org/10.1038/ncomms8321.

55. Ibrahim, A.G.E., Cheng, K., and Marbán, E. (2014). Exosomes as critical agents of cardiac regeneration triggered by cell therapy. Stem Cell Rep. *2*, 606–619. https://doi.org/10.1016/j.stemcr.2014.04.006.

56. Song, Y., Dou, H., Li, X., Zhao, X., Li, Y., Liu, D., Ji, J., Liu, F., Ding, L., Ni, Y., and Hou, Y. (2017). Exosomal miR-146a Contributes to the Enhanced Therapeutic Efficacy of Interleukin-1β-Primed Mesenchymal Stem Cells Against Sepsis. Stem Cell. *35*, 1208–1221. https://doi.org/10.1002/stem.2564.

57. Jiang, J., Xin, J., Ding, W., Shi, D., Sun, S., Guo, B., Zhou, X., Zheng, C., and Li, J. (2022). MicroRNA Profile of Human Bone Marrow Mesenchymal Stem Cells during Hepatic Differentiation and Therapy. Int. J. Med. Sci. *19*, 152–163. https://doi.org/10.7150/ijms.67639.

58. Aliotta, J.M., Pereira, M., Wen, S., Dooner, M.S., Del Tatto, M., Papa, E., Goldberg, L.R., Baird, G.L., Ventetuolo, C.E., Quesenberry, P.J., and Klinger, J.R. (2016). Exosomes induce and reverse monocrotaline-induced pulmonary hypertension in mice. Cardiovasc. Res. *110*, 319–330. https://doi.org/10.1093/cvr/cvw054.

59. Tofiño-Vian, M., Guillén, M.I., Pérez Del Caz, M.D., Castejón, M.A., and Alcaraz, M.J. (2017). Extracellular Vesicles from Adipose-Derived Mesenchymal Stem Cells Downregulate Senescence Features in Osteoarthritic Osteoblasts. Oxid. Med. Cell. Longev. *2017*, 7197598. https://doi.org/10.1155/2017/7197598.

60. Tofiño-Vian, M., Guillén, M.I., Pérez del Caz, M., Silvestre, A., and Alcaraz, M.J. (2018). Microvesicles from Human Adipose Tissue-Derived Mesenchymal Stem Cells as a New Protective Strategy in Osteoarthritic Chondrocytes. Cell. Physiol. Biochem. *47*, 11–25. https://doi.org/10.1159/000489739.

61. Platas, J., Guillén, M.I., Del Caz, M.D.P., Gomar, F., Mirabet, V., and Alcaraz, M.J. (2013). Conditioned Media from Adipose-Tissue-Derived Mesenchymal Stem Cells Downregulate Degradative Mediators Induced by Interleukin-1$\beta$in Osteoarthritic Chondrocytes. Mediat. Inflamm. *2013*, 1–10. https://doi.org/10.1155/2013/357014.

62. Kilpinen, L., Impola, U., Sankkila, L., Ritamo, I., Aatonen, M., Kilpinen, S., Tuimala, J., Valmu, L., Levijoki, J., Finckenberg, P., et al. (2013). Extracellular membrane vesicles from umbilical cord blood-derived MSC protect against ischemic acute kidney injury, a feature that is lost after inflammatory conditioning. J. Extracell. Vesicles *2*, 21927. https://doi.org/10.3402/jev.v2i0.21927.

63. Ti, D., Hao, H., Tong, C., Liu, J., Dong, L., Zheng, J., Zhao, Y., Liu, H., Fu, X., and Han, W. (2015). LPS-preconditioned mesenchymal stromal cells modify macrophage polarization for resolution of chronic inflammation via exosome-shuttled let-7b. J. Transl. Med. *13*, 308. https://doi.org/10.1186/s12967-015-0642-6.

64. Zhang, Q., Fu, L., Liang, Y., Guo, Z., Wang, L., Ma, C., and Wang, H. (2018). Exosomes originating from MSCs stimulated with TGF-β and IFN-γ promote Treg differentiation. J. Cell. Physiol. *233*, 6832–6840. https://doi.org/10.1002/jcp.26436.

65. Hwang, S., Sung, D.K., Kim, Y.E., Yang, M., Ahn, S.Y., Sung, S.I., and Chang, Y.S. (2023). Mesenchymal Stromal Cells Primed by Toll-like Receptors 3 and 4 Enhanced Anti-Inflammatory Effects against LPS-Induced Macrophages via Extracellular Vesicles. Int. J. Mol. Sci. *24*, 16264. https://doi.org/10.3390/ijms242216264.

66. Hackel, A., Aksamit, A., Bruderek, K., Lang, S., and Brandau, S. (2021). TNF-α and IL-1β sensitize human MSC for IFN-γ signaling and enhance neutrophil recruitment. Eur. J. Immunol. *51*, 319–330. https://doi.org/10.1002/eji.201948336.

67. Wang, Y., Chen, X., Cao, W., and Shi, Y. (2014). Plasticity of mesenchymal stem cells in immunomodulation: pathological and therapeutic implications. Nat. Immunol. *15*, 1009–1016. https://doi.org/10.1038/ni.3002.

68. Ren, G., Zhang, L., Zhao, X., Xu, G., Zhang, Y., Roberts, A.I., Zhao, R.C., and Shi, Y. (2008). Mesenchymal stem cell-mediated immunosuppression occurs via concerted action of chemokines and nitric oxide. Cell Stem Cell *2*, 141–150. https://doi.org/10.1016/j.stem.2007.11.014.

69. Domenis, R., Cifù, A., Quaglia, S., Pistis, C., Moretti, M., Vicario, A., Parodi, P.C., Fabris, M., Niazi, K.R., Soon-Shiong, P., and Curcio, F. (2018). Pro inflammatory stimuli enhance the immunosuppressive functions of adipose mesenchymal stem cells-derived exosomes. Sci. Rep. *8*, 13325. https://doi.org/10.1038/s41598-018-31707-9.

70. Monguió-Tortajada, M., Roura, S., Gálvez-Montón, C., Pujal, J.M., Aran, G., Sanjurjo, L., Franquesa, M.l., Sarrias, M.R., Bayes-Genis, A., and Borràs, F.E. (2017). Nanosized UCMSC-derived extracellular vesicles but not conditioned medium exclusively inhibit the inflammatory response of stimulated T cells: implications for nanomedicine. Theranostics *7*, 270–284. https://doi.org/10.7150/thno.16154.

71. Schiller, L.T., Lemus-Diaz, N., Rinaldi Ferreira, R., Böker, K.O., and Gruber, J. (2018). Enhanced Production of Exosome-Associated AAV by Overexpression of the Tetraspanin CD9. Mol. Ther. Methods Clin. Dev. *9*, 278–287. https://doi.org/10.1016/j.omtm.2018.03.008.

72. Silva-Cote, I., Cruz-Barrera, M., Cañas-Arboleda, M., Correa-Araujo, L., Méndez, L., Jagielska, J., Camacho, B., and Salguero, G. (2019). Strategy for the Generation of Engineered Bone Constructs Based on Umbilical Cord Mesenchymal Stromal Cells Expanded with Human Platelet Lysate. Stem Cells Int. *2019*, 7198215. https://doi.org/10.1155/2019/7198215.

73. Stewart, S.A., Dykxhoorn, D.M., Palliser, D., Mizuno, H., Yu, E.Y., An, D.S., Sabatini, D.M., Chen, I.S.Y., Hahn, W.C., Sharp, P.A., et al. (2003). Lentivirus-delivered stable gene silencing by RNAi in primary cells. RNA *9*, 493–501. https://doi.org/10.1261/rna.2192803.

74. Lemus-Diaz, N., Tamon, L., and Gruber, J. (2018). Dual Fluorescence Reporter Based Analytical Flow Cytometry for miRNA Induced Regulation in Mammalian Cells. Bio. Protoc. *8*, e3000. https://doi.org/10.21769/BioProtoc.3000.